# CHAPTER 3
# THE FOURIER DIFFRACTION THEOREM

## 3.1 Introduction

Fundamental to diffraction tomography is the *Fourier Diffraction Projection Theorem*, which relates the Fourier transform of the measured forward scattered data with the Fourier transform of the object. *The theorem is valid when the inhomogeneities in the object are only weakly scattering* and can be stated as [Kak84]:

> When an object, f(x,y), is illuminated with a plane wave as shown in Figure 3.1, the Fourier transform of the forward scattered fields measured on line TT' gives the values of the 2-D transform, $F(\omega_1,\omega_2)$, of the object along a circular arc in the frequency domain, as shown in the right half of the figure.

The importance of the theorem is made obvious by noting that if an object is illuminated by plane waves from many directions over $360^\circ$, the resulting circular arcs in the $(\omega_1,\omega_2)$-plane will fill the frequency domain. The function f(x,y) may then be recovered by Fourier inversion.

Before giving a short proof of the theorem, first a few words about the dimensionality of the object compared to that of the scattered fields. Although the theorem talks about a two-dimensional object, what is actually meant is an object that does not vary in the z direction. In other words, the theorem is about any cylindrical object whose cross-sectional distribution is given by the function f(x,y). The forward scattered fields are measured on a line of detectors along TT' in Figure 3.1.

If a truly three-dimensional object is illuminated by a plane wave, the forward scattered fields would now have to be measured by a planar array of detectors. The Fourier transform of the fields measured by such an array would give the values of the 3-D transform of the object over a spherical surface. This was first shown by Wolf [Wol69]. A more recent exposition is in [Nah84 and Dev84], where the authors have also presented a new synthetic

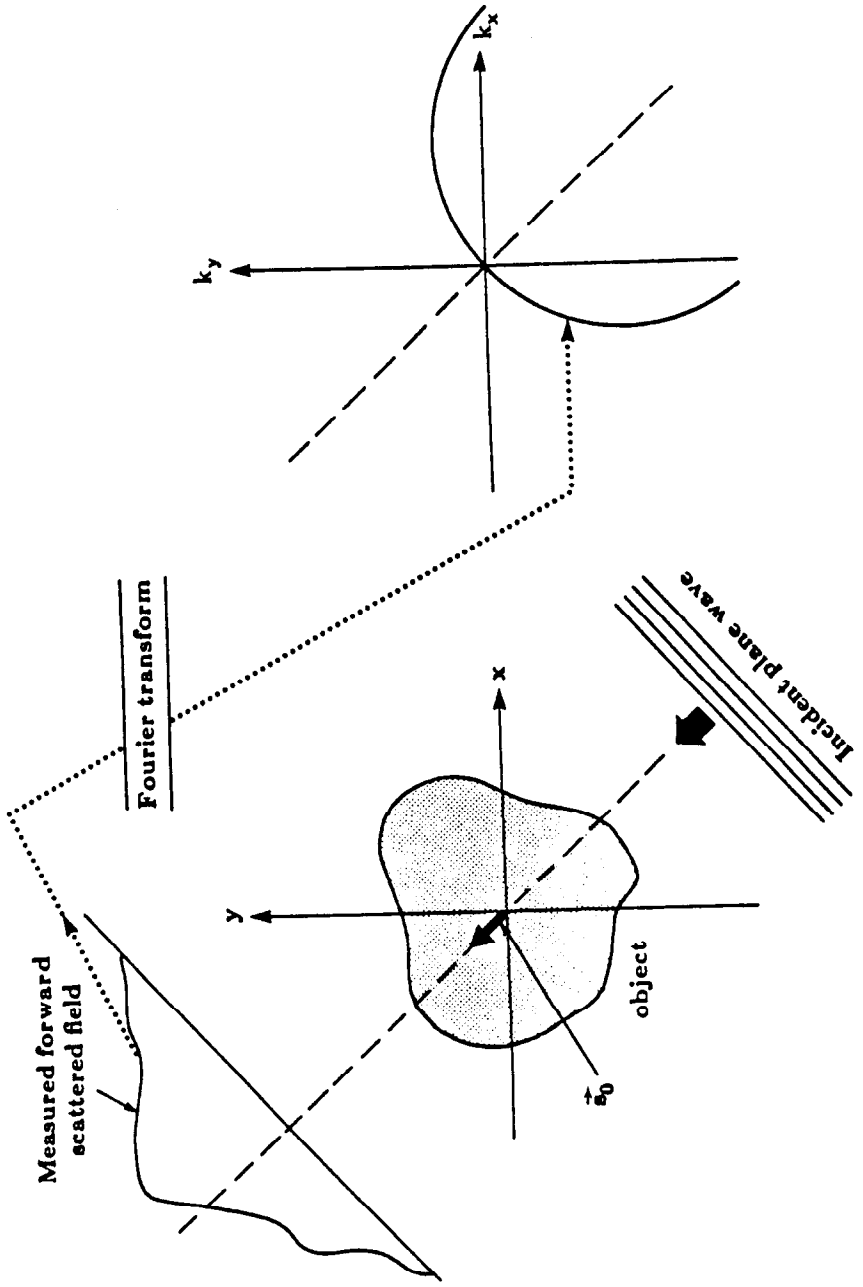


Figure 3.1 The Fourier Diffraction Theorem.

aperture procedure for a full three dimensional reconstruction using only two rotational positions of the object. This chapter, however, will continue to work with two dimensional objects in the sense described here. A recent work describing some of the errors in this approach is [LuZ84].

## 3.2 Decomposing the Green's Function

Earlier in this work, the scattered field due to a weakly scattering object was expressed as the convolution

$$u_B(\vec{r}) = \int o(\vec{r}\,')u_0(\vec{r}\,')g(\vec{r}-\vec{r}\,')d\vec{r}\,' \tag{3.1}$$

where $u_B(\vec{r})$ represents the complex amplitude of the field as in the Born approximation or the incident field, $u_0(\vec{r})$, times the complex scattered phase, $\phi_s(\vec{r})$, in the Rytov approximation. From this integral there are two approaches to the derivation of the Fourier Diffraction Theorem. Many researchers [Mue79, Gre78, Dev82] have expanded the Green's function into its plane wave decomposition and then noticed the similarity of the resulting expression and the Fourier transform of the object. Alternatively, if the Fourier transform of each component of this equation (3.1) is taken then the Fourier Diffraction Theorem can be derived in a manner that can be easily visualized and points towards efficient computer implementations. This work will present both approaches to the derivation of the Fourier Diffraction Theorem: the first because the math is more straightforward, the second because it provides more insight into the difference between transmission and reflection tomography.

First the Green's function will be decomposed into its plane wave components.

### 3.2.1 Plane Wave Approach

The integral equation for the scattered field (3.1) can be considered as a convolution of the Green's Function, $g(\vec{r}-\vec{r}\,')$, and the product of the object function, $o(\vec{r}\,')$, and the incident field, $u_0(\vec{r}\,')$. Consider the effect of a single plane wave illuminating an object. The forward scattered field will be measured at the receiver line as is shown in Figure 3.2.

A single plane wave in two dimensions can be represented as

$$u_0(\vec{r}) = e^{j\vec{K}\cdot\vec{r}} \tag{3.2}$$

where $\vec{K} = (k_x,k_y)$ satisfies the following relationship

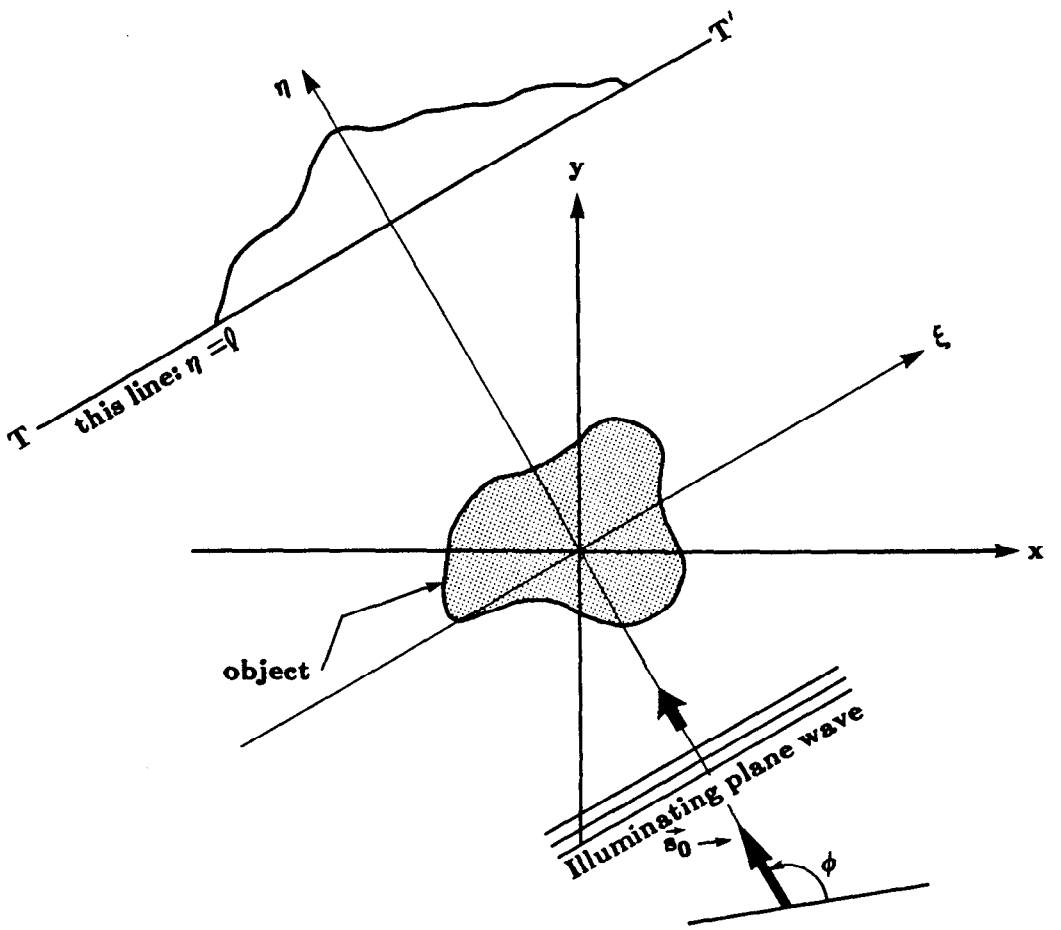


Figure 3.2 A typical diffraction tomography experiment

$$k_0^2 = k_x^2 + k_y^2. \tag{3.3}$$

From earlier in this work, the two dimensional Green's function is given by

$$g(\vec{r}|\vec{r}') = \frac{j}{4} H_0(k_0|\vec{r}-\vec{r}'|) \tag{3.4}$$

and $H_0$ is the zero-order Hankel function of the first kind. The function $H_0$ has the plane wave decomposition [Mor53]

$$H_0(k|\vec{r}-\vec{r}'|) = \frac{1}{\pi}\int_{-\infty}^{\infty} \frac{1}{\beta} e^{j[\alpha(x-x')+\beta|y-y'|]} d\alpha \tag{3.5}$$

where $\vec{r} = (x,y)$, $\vec{r}' = (x',y')$ and

$$\beta = \sqrt{k_0^2-\alpha^2}. \tag{3.6}$$

Basically, equation (3.5) expresses a cylindrical wave, $H_0$, as a superposition of plane waves. At all points, the wave centered at $\vec{r}'$ is traveling outward; for points such that $y>y'$ the plane waves propagate upward while for $y<y'$ the plane waves propagate downward. In addition, for $|\alpha| \leq k_0$, the plane waves are of the ordinary type, propagating along the direction given by $\tan^{-1}(\beta/\alpha)$. However, for $|\alpha| > k_0$, $\beta$ becomes imaginary, the waves decay exponentially and they are called *evanescent waves.* Evanescent waves are usually of no significance beyond about 10 wavelengths from the source.

Substituting this expression, (3.5), into the expression for the scattered field, (3.1), the scattered field can now be written

$$u_B(\vec{r}) = \frac{j}{4\pi}\int o(\vec{r}')u_0(\vec{r}')\int_{-\infty}^{\infty} \frac{1}{\beta} e^{j[\alpha(x-x')+\beta|y-y'|]} d\alpha d\vec{r}' \tag{3.7}$$

In order to show the first steps in the proof of this theorem, assume for notational convenience that the direction of the incident plane wave is along the positive y-axis. Thus the incident field is given by

$$u_0(\vec{r}) = e^{j\vec{s}_0\cdot\vec{r}} \tag{3.8}$$

where $\vec{s}_0 = (0,k_0)$. Since in transmission imaging the scattered fields are measured by a linear array located at $y = l_0$, where $l_0$ is greater than any y-coordinate within the object (see Figure 3.2), the term $|y-y'|$ in the above expression may simply be replaced by $l_0-y'$ and the resulting form may be rewritten

$$u_B(x,y=l_0) = \frac{j}{4\pi}\int_{-\infty}^{\infty} d\alpha \int \frac{o(\vec{r}')}{\beta} e^{j[\alpha(x-x')+\beta(l_0-y')]} e^{jk_0 y'} d\vec{r}' \qquad (3.9)$$

Recognizing part of the inner integral as the two-dimensional Fourier transform of the object function evaluated at a frequency of $(\alpha,\beta-k_0)$ the scattered field can be written

$$u_B(x,y=l_0) = \frac{j}{4\pi}\int_{-\infty}^{\infty} \frac{1}{\beta} e^{j(\alpha x+\beta l_0)} O(\alpha,\beta-k_0) d\alpha \qquad (3.10)$$

where O has been used to designate the two dimensional Fourier transform of the object function.

Let $U_B(\omega,l_0)$ denote the Fourier transform of the one dimensional scattered field, $u_B(x,l_0)$, with respect to x, that is

$$U_B(\omega,l_0) = \int_{-\infty}^{\infty} u_B(x,l_0) e^{-j\omega x} dx \qquad (3.11)$$

As mentioned before, the physics of wave propagation dictate that the highest angular spatial frequency in the measured scattered field on the line $y=l_0$ is unlikely to exceed $k_0$. Therefore, in almost all practical situations, $U_s(\omega,l_0) = 0$ for $|\omega| > k_0$. This is consistent with neglecting the evanescent modes as described earlier.

If the Fourier transform of the scattered field is found by substituting equation (3.10) into equation (3.11) then using the following property of Fourier integrals

$$\int_{-\infty}^{\infty} e^{j(\omega-\alpha)x} dx = 2\pi\delta(\omega-\alpha) \qquad (3.12)$$

where $\delta(\cdot)$ is the Dirac delta function discussed in Chapter 2 the scattered field can be written

$$U_B(\alpha,l_0) = \frac{j}{2\sqrt{k_0^2-\alpha^2}} e^{j\sqrt{k_0^2-\alpha^2}\,l_0} O(\alpha,\sqrt{k_0^2-\alpha^2}-k_0) \qquad (3.13)$$

$$\text{for } |\alpha| < k_0.$$

This expression relates the two dimensional Fourier transform of the object to the one dimensional Fourier transform of the field at the receiver line. The factor

$$\frac{j}{2\sqrt{k_0^2-\alpha^2}} e^{j\sqrt{k_0^2-\alpha^2}l_0} \tag{3.14}$$

is a simple constant for a fixed receiver line. As $\alpha$ varies from $-k_0$ to $k_0$, the coordinates $(\alpha, \sqrt{k_0^2-\alpha^2}-k_0)$ in the Fourier transform of the object function trace out a semicircular arc in the (u,v)-plane as shown in Figure 3.1. This proves the Fourier Diffraction Theorem.

To summarize, if the Fourier transform of the forward scattered data is found when the incident illumination is propagating along the positive y-axis, the resulting transform will be zero for angular spatial frequencies $|\alpha| > k_0$. For $|\alpha| < k_0$, the transform of the data gives values of the Fourier transform of the object on the semicircular arc are shown in Figure 3.1 in the (u,v)-plane. The endpoints A and B of the semicircular arc are at a distance of $\sqrt{2}k_0$ from the origin in the frequency domain.

### 3.2.2 Fourier Transform Approach

Another approach to the derivation of the Fourier Diffraction Theorem is possible if the scattered field

$$u_B(\vec{r}) = \int o(\vec{r}\,')u_0(\vec{r}\,')g(\vec{r}-\vec{r}\,')d\vec{r}\,' \tag{3.15}$$

is considered entirely in the Fourier domain. The plots of Figure 3.3 will be used to illustrate the various transformations that take place.

Again consider the effect of a single plane wave illuminating an object. The forward scattered field will be measured at the receiver line as is shown in Figure 3.2.

The integral equation for the scattered field can be considered as a convolution of the Green's Function, $g(\vec{r}-\vec{r}\,')$, and the product of the object function, $o(\vec{r}\,')$, and the incident field, $u_0(\vec{r}\,')$. First define the following Fourier transform pairs.

$$o(\vec{r}) \leftrightarrow O(\vec{K})$$

$$g(\vec{r}-\vec{r}\,') \leftrightarrow G(\vec{K}) \tag{3.16}$$

$$u(\vec{r}) \leftrightarrow U(\vec{K})$$

The integral solution to the wave equation can now be written in terms of these Fourier transforms or

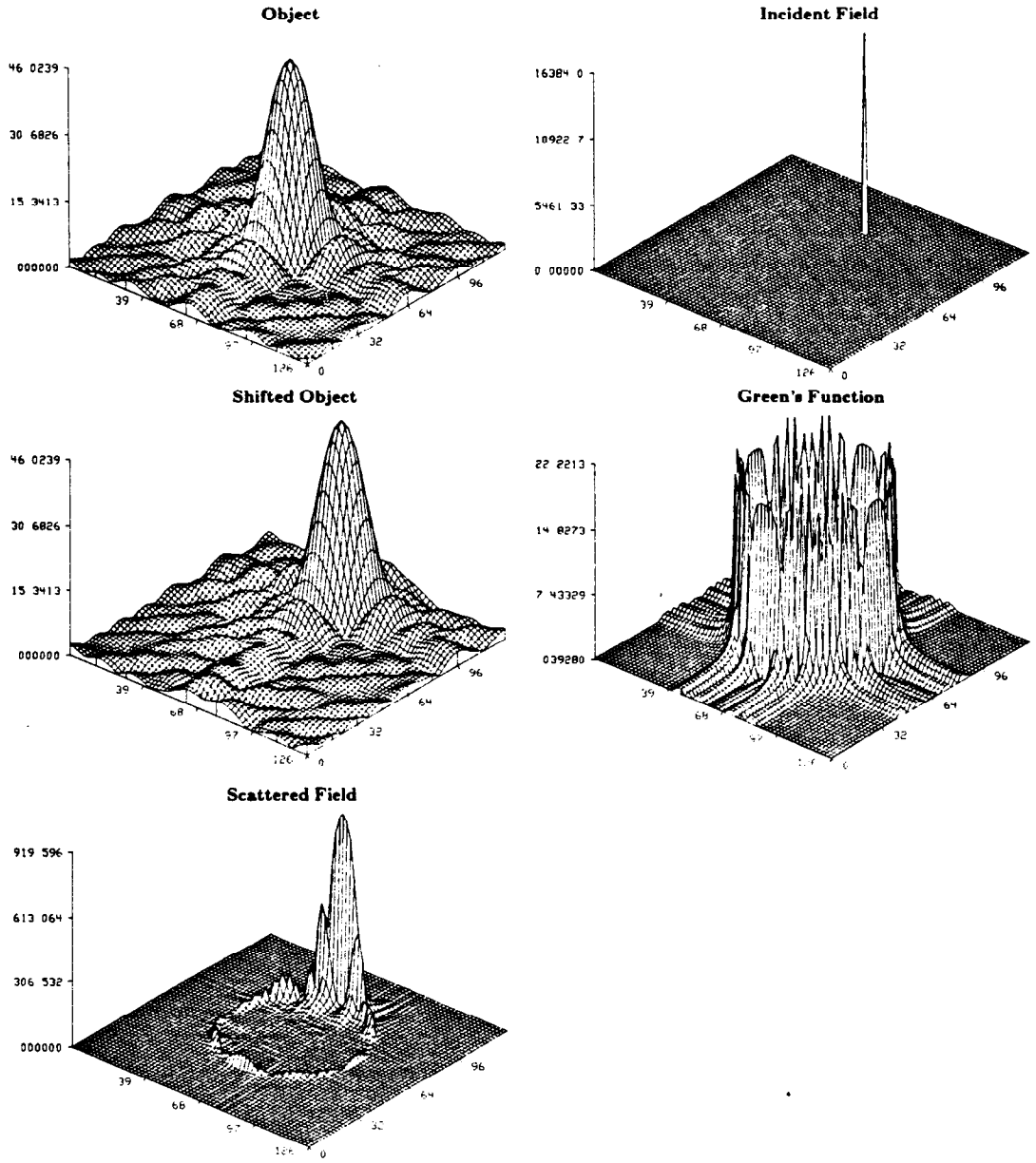


Figure 3.3 Two dimensional Fourier representation of the Helmholtz equation. (a) The object, (b) the incident field, (c) the Green's function, (d) the (space domain) product of the object and the incident field and (e) the two dimensional Fourier transform of the scattered field.

$$U_s(\vec{\Lambda}) = G(\vec{\Lambda})\left\{O(\vec{\Lambda})*U_0(\vec{\Lambda})\right\} \tag{3.17}$$

where '*' has been used to represent convolution and $\vec{\Lambda} = (\alpha,\gamma)$. In equation (3.2) an expression for $u_0$ was presented. It's Fourier transform is given by

$$U_0(\vec{\Lambda}) = 2\pi\delta(\vec{\Lambda}-\vec{K}) \tag{3.18}$$

and thus the convolution of equation (3.17) becomes a shift in the frequency domain or

$$O(\vec{\Lambda})*U_0(\vec{\Gamma}) = 2\pi O(\vec{\Lambda}-\vec{K}). \tag{3.19}$$

This convolution is illustrated in Figures 3.3a-c for a plane wave propagating with direction vector, $\vec{K} = (0,k_0)$. Figure 3.3a shows the Fourier transform of a single cylinder of radius $1\lambda$ and Figure 3.3b is the Fourier transform of the incident field. The resulting multiplication in the space domain or convolution in the frequency domain is shown in Figure 3.3c.

To find the Fourier transform of the Green's function the Fourier transform of the equation for a point scatterer

$$(\nabla^2+k_0^2)g(\vec{r}\,|\,\vec{r}\,') = -\delta(\vec{r}-\vec{r}\,'), \tag{3.20}$$

is taken to find

$$(-\Lambda^2+k_0^2)G(\vec{\Lambda}\,|\,\vec{r}\,') = -e^{-j\vec{\Lambda}\cdot\vec{r}\,'}. \tag{3.21}$$

Rearranging terms the following expression for the Fourier transform of the Green's function is found

$$G(\vec{\Lambda}\,|\,\vec{r}\,') = \frac{e^{-j\vec{\Lambda}\cdot\vec{r}}}{\Lambda^2-k_0^2}. \tag{3.22}$$

This has a singularity for all $\vec{\Lambda}$ such that

$$|\Lambda|^2 = \alpha^2+\gamma^2 = k_0^2. \tag{3.23}$$

An approximation to $G(\vec{\Lambda})$ is shown in Figure 3.3d.

The Fourier transform representation is misleading because it represents a point scatterer as both a sink and a source of waves. A single plane wave propagating from left to right can be considered in two different ways depending on the point of view. From the left side of the scatter, the point scatterer represents a sink to the wave while to the right of the scatterer the

wave is spreading from a source point. Clearly, it is not possible for a scatterer to be both a point source and sink, and later when our expression for the scattered field is inverted, it will be necessary to choose a solution that leads to outgoing waves only.

The effect of the convolution shown in equation (3.15) is a multiplication in the frequency domain of the shifted object function, (3.19), and the Green's function, (3.22), evaluated at $\vec{r}' = 0$. The scattered field is written as

$$U_s(\vec{\Lambda}) = 2\pi \frac{O(\vec{\Lambda}-\vec{K})}{\Lambda^2-k^2}. \tag{3.24}$$

This result is shown in Figure 3.3e for a plane wave propagating along the y-axis. Since the largest frequency domain components of the Green's function satisfy equation (3.23), the Fourier transform of the scattered field is dominated by a shifted and sampled version of the object's Fourier transform.

An expression for the field at the receiver line will now be derived. For simplicity it will continue to be assumed that the incident field is propagating along the positive y axis or $\vec{K} = (0,k_0)$. The scattered field along the receiver line $(x,y=l_0)$ is simply the inverse Fourier transform of the field in equation (3.24). This is written as

$$u(x,y=l_0) = \frac{1}{4\pi^2} \int_{-\infty}^{\infty}\int_{-\infty}^{\infty} U_s(\vec{\Lambda}) e^{j\vec{\Lambda}\cdot\vec{r}} d\alpha d\gamma \tag{3.25}$$

which, using (3.24), can be expressed as

$$u_s(x,y=l_0) = \frac{1}{4\pi^2} \int_{-\infty}^{\infty}\int_{-\infty}^{\infty} \frac{O(\alpha,\gamma-k_0)}{\alpha^2+\gamma^2-k_0^2} e^{j(\alpha x+\gamma l_0)} d\alpha d\gamma. \tag{3.26}$$

First find the integral with respect to $\gamma$. For a given $\alpha$, the integral has a singularity for

$$\gamma_{1,2} = \pm\sqrt{k_0^2-\alpha^2} \tag{3.27}$$

Using contour integration the integral can be evaluated with respect to $\gamma$ along the path shown in Figure 3.4. By adding $\frac{1}{2\pi}$ of the residue at each pole the scattered field is expressed

$$u_s(x,y) = \frac{1}{2\pi}\int \Gamma_1(\alpha;y) e^{j\alpha x} d\alpha + \frac{1}{2\pi}\int \Gamma_2(\alpha;y) e^{j\alpha x} d\alpha \tag{3.28}$$

where

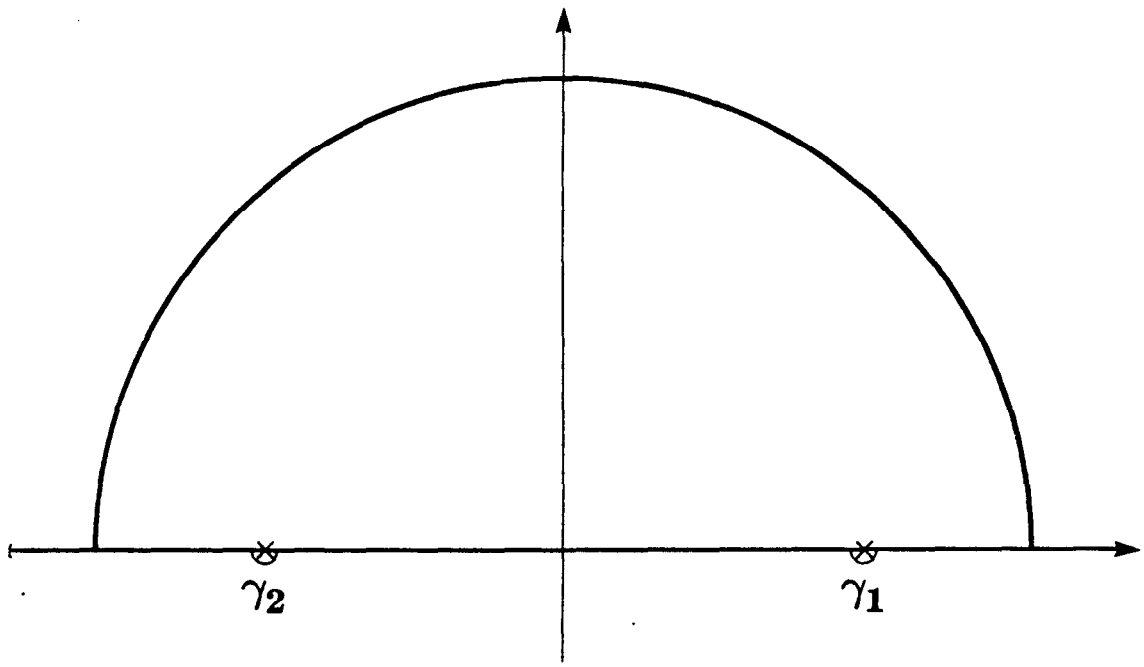


Figure 3.4 Integration path in the complex plane for inverting the two dimensional Fourier transform of the scattered field.

$$\Gamma_1 = \frac{jO(\alpha, \sqrt{k_0^2-\alpha^2}-k_0)}{2\sqrt{k_0^2-\alpha^2}} e^{j\sqrt{k_0^2-\alpha^2}l_0} \tag{3.29}$$

and

$$\Gamma_2 = \frac{-jO(\alpha, -\sqrt{k_0^2-\alpha^2}-k_0)}{2\sqrt{k_0^2-\alpha^2}} e^{-j\sqrt{k_0^2-\alpha^2}l_0} \tag{3.30}$$

Examining the above pair of equations it can be seen that $\Gamma_1$ represents the solution in terms of plane waves traveling along the positive y axis while $\Gamma_2$ represents plane waves traveling in the $-y$ direction.

As was discussed earlier, the Fourier transform of the Green's function (3.22) represents the field due to both a point source and a point sink but the two solutions are distinct for receiver lines that are outside the extant of the object. First consider the scattered field along the line $y = l_0$ where $l_0$ is greater than the y-coordinate of all points in the object. Since all scattered fields originate in the object, plane waves propagating along the positive y axis represent outgoing waves while waves propagating along the negative y axis represent waves due to a point sink. Thus for y>object (i.e. the receiver line is above the object) the outgoing scattered waves are represented by $\Gamma_1$ or

$$u_s(x,y) = \frac{1}{2\pi}\int \Gamma_1(\alpha;y) e^{j\alpha x} d\alpha \qquad y>\text{object} \tag{3.31}$$

Conversely for a receiver along a line $y = l_0$ where $l_0$ is less than the y-coordinate of any point in the object the scattered field is represented by $\Gamma_2$ or

$$u_s(x,y) = \frac{1}{2\pi}\int \Gamma_2(\alpha;y) e^{j\alpha x} d\alpha \qquad y<\text{object} \tag{3.32}$$

In general the scattered field will be written as as

$$u_s(x,y) = \frac{1}{2\pi}\int \Gamma(\alpha;y) e^{j\alpha x} d\alpha \tag{3.33}$$

and it will be understood that values of the square root in the expression for $\Gamma$ should be chosen that lead only to outgoing waves.

Taking the Fourier transform of both sides of equation (3.33) the Fourier transform of the scattered field at the receiver line is written

$$\int u(x,y=l_0) e^{-j\alpha x} dx = \Gamma(\alpha, l_0). \tag{3.34}$$

But since by equations (3.29) and (3.30), $\Gamma(\alpha, l_0)$ is equal to a phase shifted version of the object function then the Fourier transform of the scattered field

along the line $y=l_0$ is related to the Fourier transform of the object along a circular arc. The use of the contour integration is further justified by noting that only those waves that satisfy the relationship

$$\alpha^2+\gamma^2 = k_0^2 \tag{3.35}$$

will be propagated and thus it is safe to ignore all waves not on the $k_0$-circle.

This result is diagramed in Figure 3.5. The circular arc represents the locus of all points $(\alpha,\gamma)$ such that $\gamma = \pm\sqrt{k_0^2-\alpha^2}$. The solid line shows the outgoing waves for a receiver line at $y=l_0$ above the object. This can be considered transmission tomography. Conversely the dashed line indicates the locus of solutions for the reflection tomography case, or $y=l_0$ is below the object.

### 3.3 Limit of the Fourier Diffraction Theorem

While at first the derivations of the Fourier Slice Theorem and the Fourier Diffraction Theorem seem quite different, it is interesting to note that in the limit of very high energy waves or, equivalently, very short wavelengths the Fourier Diffraction Theorem is closely approximated by the Fourier Slice Theorem. Recall that the Fourier transform of a diffracted projection corresponds to samples of the two dimensional Fourier transform of an object along a circular arc. As shown in Figure 3.1 the radius of the arc is equal to $k_0$ which is given by

$$k_0 = \frac{2\pi}{\lambda} \tag{3.36}$$

and $\lambda$ is the wavelength of the energy. As the wavelength is decreased, the wavenumber, $k_0$, and the radius of the arc in the object's Fourier domain grows. This process is illustrated in Figure 3.6 where the semicircular arc resulting from a diffraction experiment is shown at six different frequencies.

An example might make this idea clearer. Compare an ultrasonic diffraction apparatus and a typical x-ray scanner. The ultrasonic experiment might be carried out at a frequency of 5 MHz and a wavelength in water of .3 mm. This corresponds to a $k_0$ of 333 radians/meter. On the other hand, an x-ray source with a 100 keV beam has a wavelength of .012 $\mu$M. The result is that a diffraction experiment gives samples along an arc of radius $5\text{x}10^8$ radians/meter. Certainly for all physiological features (i.e. resolutions of $<$ 1000 radians/meter) the arc can be considered a straight line and the Fourier Slice Theorem is an excellent model of the propagation of x-rays.

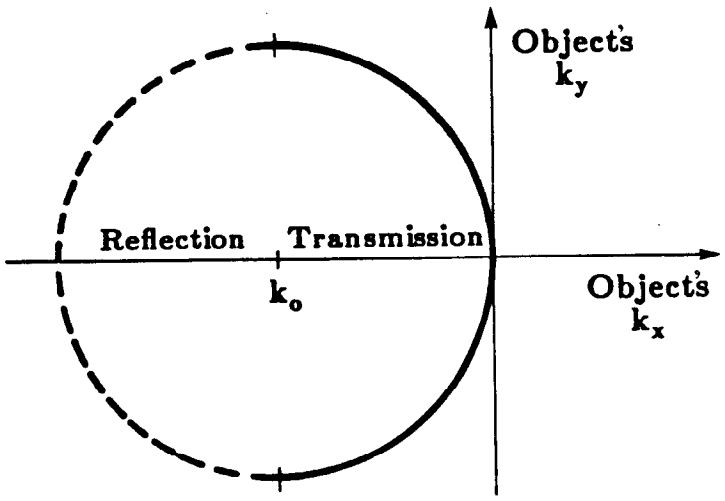


Figure 3.5 Estimate of the two dimensional Fourier transform of the object are available along the solid arc for transmission tomography and the dashed arc for reflection tomography.

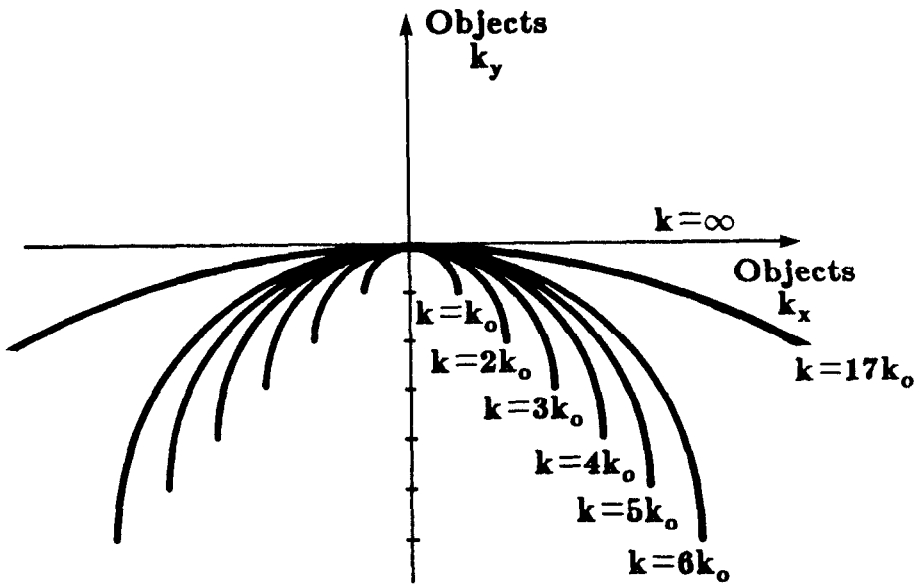


Figure 3.6 As the illuminating frequency is increased the Fourier Diffraction Theorem becomes equivalent to the Fourier Slice Theorem.

### 3.4 The Data Collection Process

The best that can be hoped for in any tomographic experiment is to estimate the Fourier transform of the object for all frequencies within a disk centered at the origin. For objects that do not have any frequency content outside the disc then the reconstruction procedure is perfect.

There are several different procedures that can be used to estimate the object function from the scattered field. A single plane wave provides exact information (up to a frequency of $\sqrt{2}k_0$) about the Fourier transform of the object along a circular arc. Two of the simplest procedures involve changing the orientation and frequency of the incident plane waves to move the frequency domain arcs to a new position. By appropriately choosing an orientation and a frequency it is possible to estimate the Fourier transform of the object at any given frequency. In, addition it is possible to change the radius of the semicircular arc by varying the frequency of the incident field and thus generating an estimate of the entire Fourier transform of the object.

#### 3.4.1 Plane Wave Illumination

The most straightforward data collection procedure consists of rotating the object and measuring the scattered field for different orientations. Each orientation will produce an estimate of the object's Fourier transform along a circular arc and these arcs will rotate as the object is rotated. When the object is rotated through a full 360 degrees an estimate of the object will be available for the entire Fourier disk.

The coverage for this method is shown in Figure 3.7 for a simple experiment with 8 projections of 9 samples each. Notice that there are two arcs that pass through each point of Fourier space. Generally it will be necessary to choose one estimate as better.

On the other hand if the reflected data is collected by measuring the field on the same side of the object as the source then estimates of the object are available for frequencies greater than $\sqrt{2}k_0$. This follows from Figure 3.5.

The first experimental results for diffraction tomography were presented by Carter and Ho [Car70, Car74, Car76 and Ho76]. They used an optical plane wave to illuminate a small glass object and were able to measure the scattered fields using a hologram. Later a group of researchers at the University of Minnesota carried out the same experiments using ultrasound and gelatine phantoms. Their results are discussed in [Kav82].

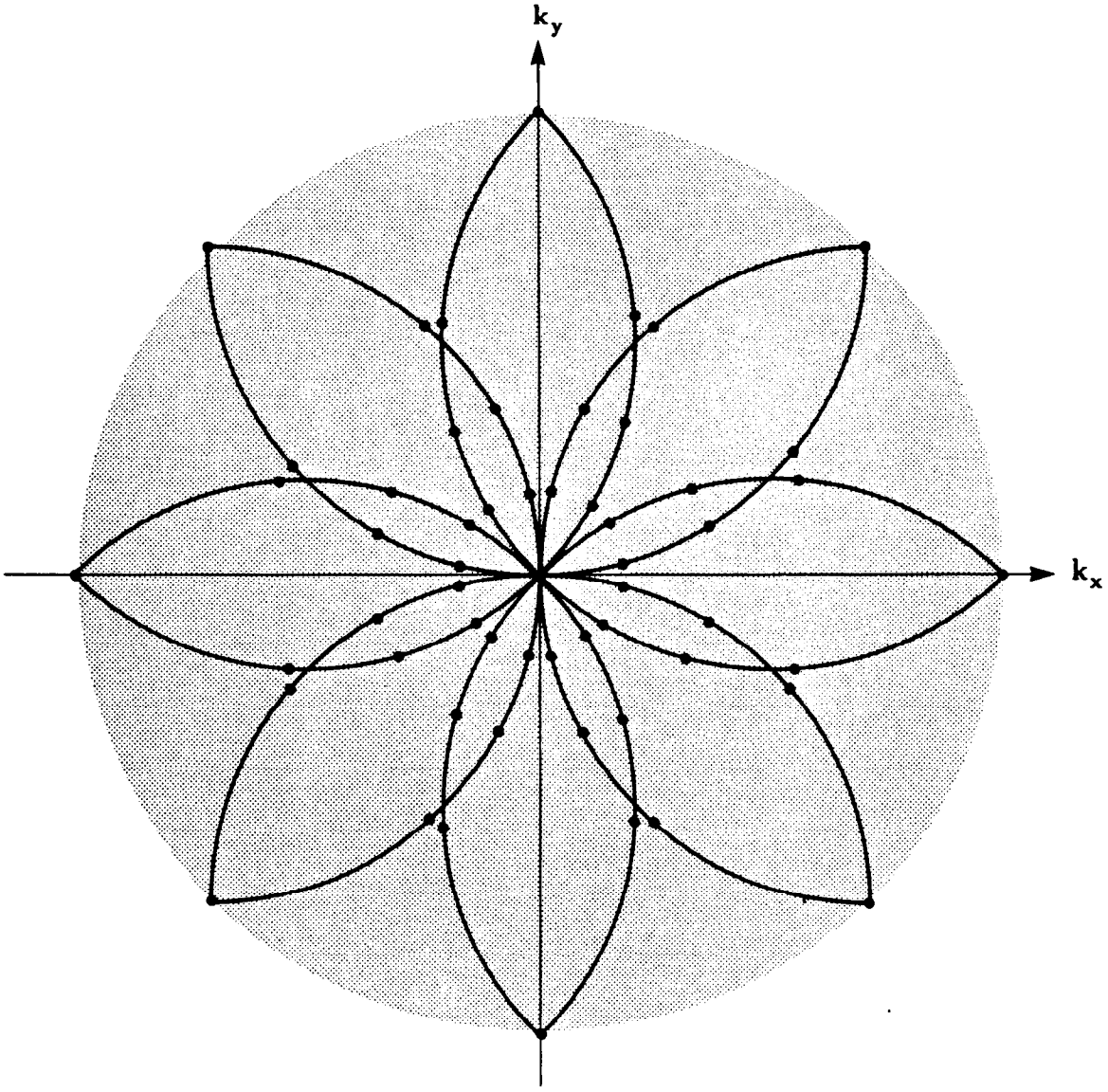


Figure 3.7 Estimates of the object's two dimensional Fourier transform are available along the circular arcs for plane wave illumination.

### 3.4.2 Synthetic Aperture

Nahamoo and Kak [Nah82, Nah84] and Devaney [Dev84] have proposed a method that requires only two rotational views of an object. Consider an arbitrary source of waves in the transmitter plane as shown in Figure 3.8. The transmitted field, $u_t$, can be represented as a weighted set of plane waves by taking the Fourier transform of the transmitter aperture function [Goo68]. Doing this the transmitted field can be expressed as

$$u_t(x) = \frac{1}{4\pi^2}\int_{-\infty}^{\infty} A_t(k_x)e^{jk_x x}dk_x. \tag{3.37}$$

Moving the source to a new position, $\eta$, the plane wave decomposition of the transmitted field becomes

$$u_t(x;\eta) = \frac{1}{4\pi^2}\int_{-\infty}^{\infty}\left(A_t(k_x)e^{jk_x\eta}\right)e^{jk_x x}dk_x. \tag{3.38}$$

Given the plane wave decomposition, the incident field in the plane follows simply as

$$u_i(\eta;x,y) = \int_{-\infty}^{\infty}\left(\frac{1}{4\pi^2}A_t(k_x)e^{jk_x\eta}\right)e^{j(k_x x + k_y y)}dk_x. \tag{3.39}$$

In equation (3.34) an equation for the scattered field from a single plane wave was presented. Because of the linearity of the Fourier transform, the effect of each plane wave, $e^{j(k_x x + k_y y)}$, can be weighted by the expression in brackets above and superimposed to find the Fourier transform of the total scattered field due to the incident field $u_t(x;\eta)$ as [Nah82]

$$U_s(\eta;\alpha) = \int_{-\infty}^{\infty}\left(A_t(k_x)e^{jk_x\eta}\right)\frac{O(\alpha-k_x,\gamma-k_y)}{j2\gamma}dk_x. \tag{3.40}$$

Taking the Fourier transform of both sides with respect to the transmitter position, $\eta$, the Fourier transform of the scattered field with respect to both the transmitter and the receiver position is given by

$$U_s(k_x;\alpha) = A_t(k_x)\frac{O(\alpha-k_x,\gamma-k_y)}{j2\gamma}k_x. \tag{3.41}$$

This approach gets the name synthetic aperture because a phase is added to the field measured for each transmitter position to synthesize a transmitted plane wave. Thus this method has a lot in common with the theory of phased arrays. Figure 3.9 shows that by properly phasing the wave transmitted at each transmitter location a plane wave can be generated that travels in an

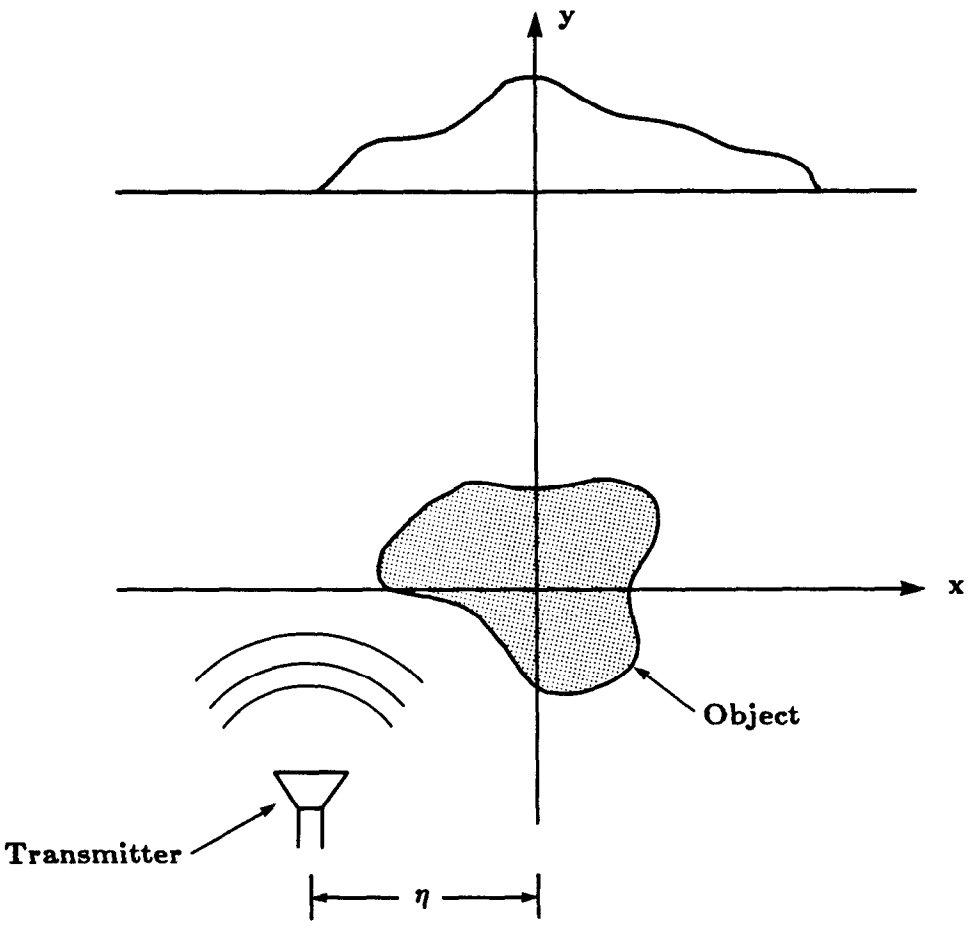


Figure 3.8 A typical synthetic aperture tomography experiment.

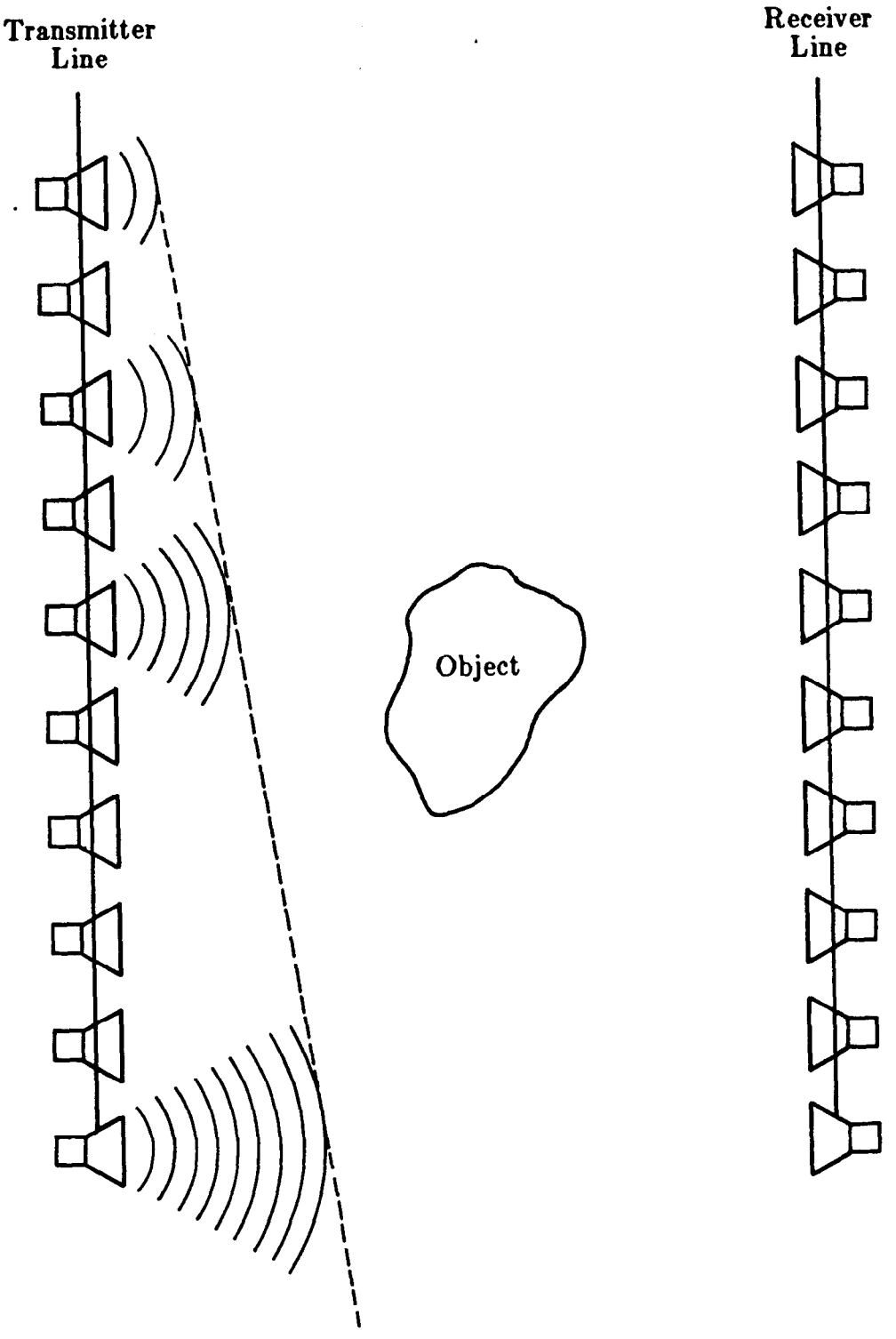


Figure 3.9 By adding a phase to the field transmitted from each transmitter any desired plane wave can be synthesized.

arbitrary direction. Since the system is linear it doesn't matter whether the phase is added to the transmitted signal or as part of the reconstruction procedure. Thus multiplying the received field for each transmitter position by the pure phase term $e^{jk_x\eta}$, where $\eta$ represents the location of the transmitter, is equivalent to an experiment with an incident plane wave with the direction vector $(k_x, \sqrt{k_0^2-k_x^2})$.

By collecting the scattered field along the receiver line as a function of transmitter position, $\eta$, an expression can be written for the scattered field. Like the simpler case with plane wave incidence, the scattered field is related to the Fourier transform of the object along an arc. Unlike the previous case, though, the coverage due to a single view of the object is a pair of circular disks as shown in Figure 3.10. Here a single view consists of transmitting from all positions in a line and measuring the scattered field at all positions along the receiver line. By rotating the object by 90 degrees it is possible to generate the complimentary disk and to fill the Fourier domain.

The coverage shown in Figure 3.10 is constructed by calculating $(\vec{K}-\vec{\Lambda})$ for all vectors $(\vec{K})$ and $(\vec{\Lambda})$ that satisfy the experimental constraints. Not only must each vector satisfy the wave equation but it is also necessary that only forward traveling plane waves be used. The dashed line in Figure 3.10 shows the valid propagation vectors $(-\vec{\Lambda})$ for the transmitted waves. To each possible vector $(-\vec{\Lambda})$ a semicircular set of vectors representing each possible received wave can be added. The locus of received plane waves is shown as a solid semi-circle centered at each of the transmitted waves indicated by an 'x'. The entire coverage for the synthetic aperture approach is shown as the shaded areas.

In addition to the diffraction tomography configurations proposed by Mueller and Nahamoo other approaches have been proposed. In Vertical Seismic Profiling (VSP) [Dev84] the scattering between the surface of the Earth and a borehole is measured. Alternately a broadband incident field can be used to illuminate the object. In both cases, the goal is to estimate the Fourier transform of the object.

In geophysical imaging it is not possible to generate or receive waves from all positions around the object. If it is possible to drill a borehole then it is possible to perform VSP and obtain information about most of the object. A typical experiment is shown in Figure 3.11. So as to not damage the borehole, acoustic waves are generated at the surface using acoustic detonators or other methods and the scattered field is measured in the borehole.

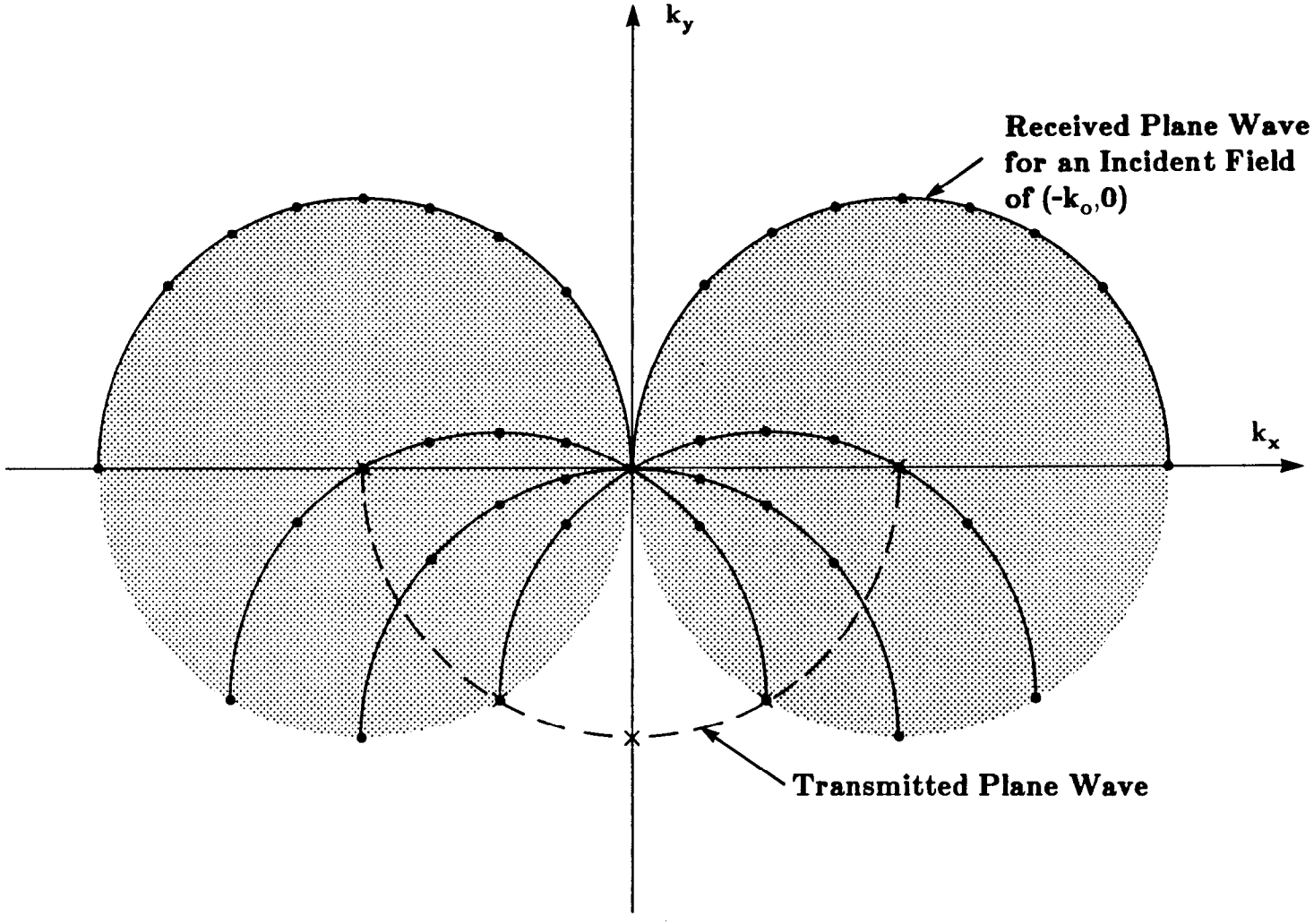


Figure 3.10 Estimates of the Fourier transform of an object in a synthetic aperture experiment are available in the shaded region.

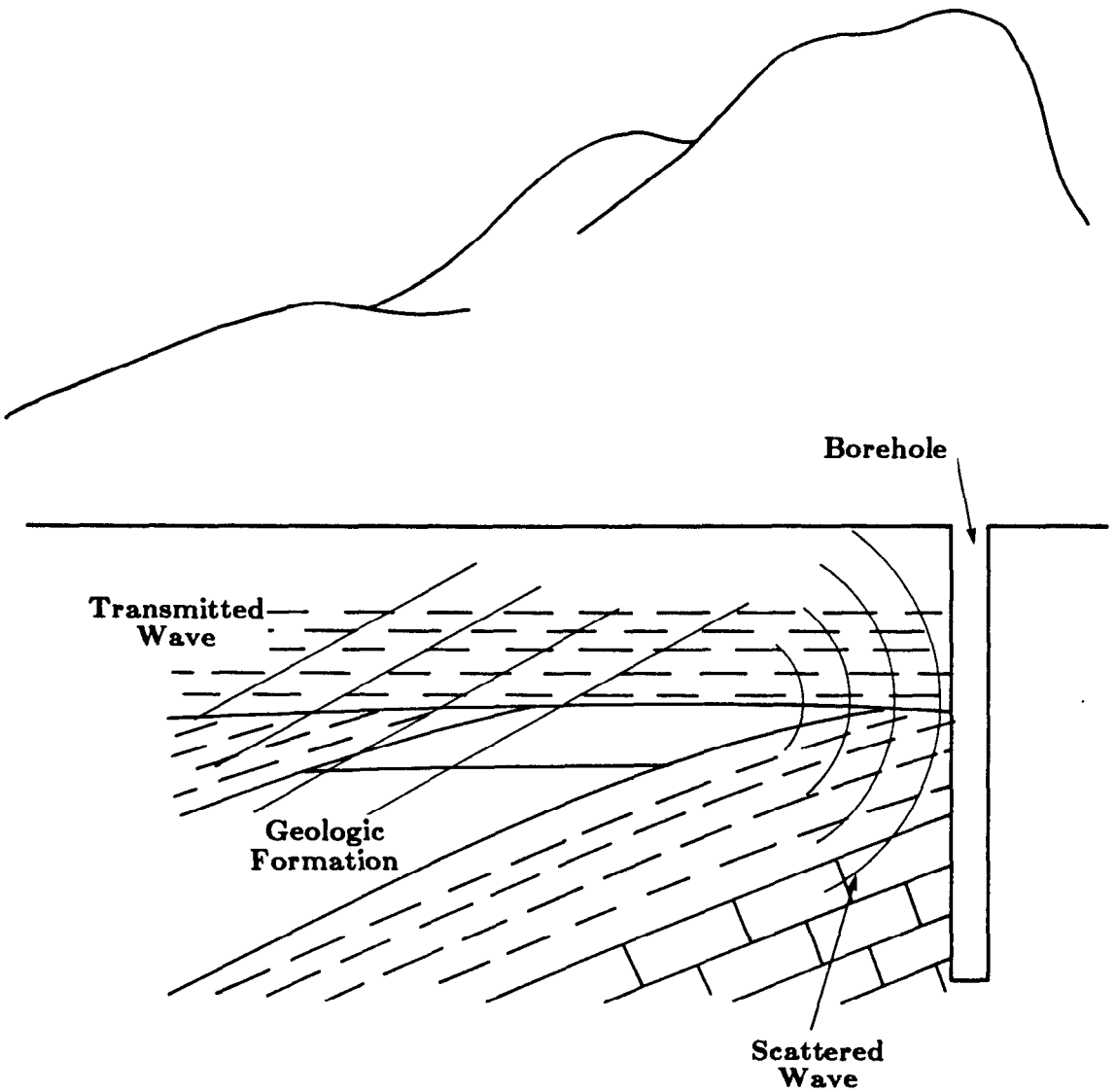


Figure 3.11 A typical Vertial Seismic Profiling (VSP) experiment.

The coverage in the frequency domain is similar to the synthetic aperture approach. Plane waves at an arbitrary downward direction are synthesized by appropriately phasing the transmitting transducers. The receivers will receive any waves traveling to the right. The resulting coverage for this method is shown in Figure 3.12a. If can be assumed that the object function is real valued then the symmetry of Fourier transform for real valued functions can be used to obtain the coverage in Figure 3.12b.

### 3.4.3 Broadband Illumination

It is also possible to perform an experiment for broadband illumination [Ken82]. Up until this point only narrow band illumination has been considered; wherein the field at each point can be completely described by its complex amplitude.

Now consider a transducer that illuminates an object with a wave of the form $a_t(k_k,t)$. Taking the Fourier transform in the time domain this wave can be decomposed into a number of experiments. Let

$$A_t(k_x,\omega) = \int_{-\infty}^{\infty} a_t(k_x,t)e^{-j\omega t}dt \tag{3.42}$$

where $\omega$ is related to $k_\omega$ by

$$k_\omega = \frac{c}{\omega}, \tag{3.43}$$

c is the speed of propagation in the media and the wavevector $(k_x,k_y)$ satisfies the wave equation

$$k_x^2+k_y^2 = k_\omega^2. \tag{3.44}$$

If a plane wave illumination of spatial frequency $k_x$ and a temporal frequency $\omega$ leads to the scattered field $u_s(k_x,w;y)$ then the total scattered field is given by a weighted superposition of the scattered fields or

$$u_s(k_x;y) = \int_{-\infty}^{\infty} A_t(k_x,\omega)u_s(k_x,\omega;y)d\omega. \tag{3.45}$$

For plane wave incidence the coverage for this method is shown in Figure 3.13a. Figure 3.13b shows that by doing four experiments at 0, 90, 180 and 270 degrees it is possible to gather information about the entire object.

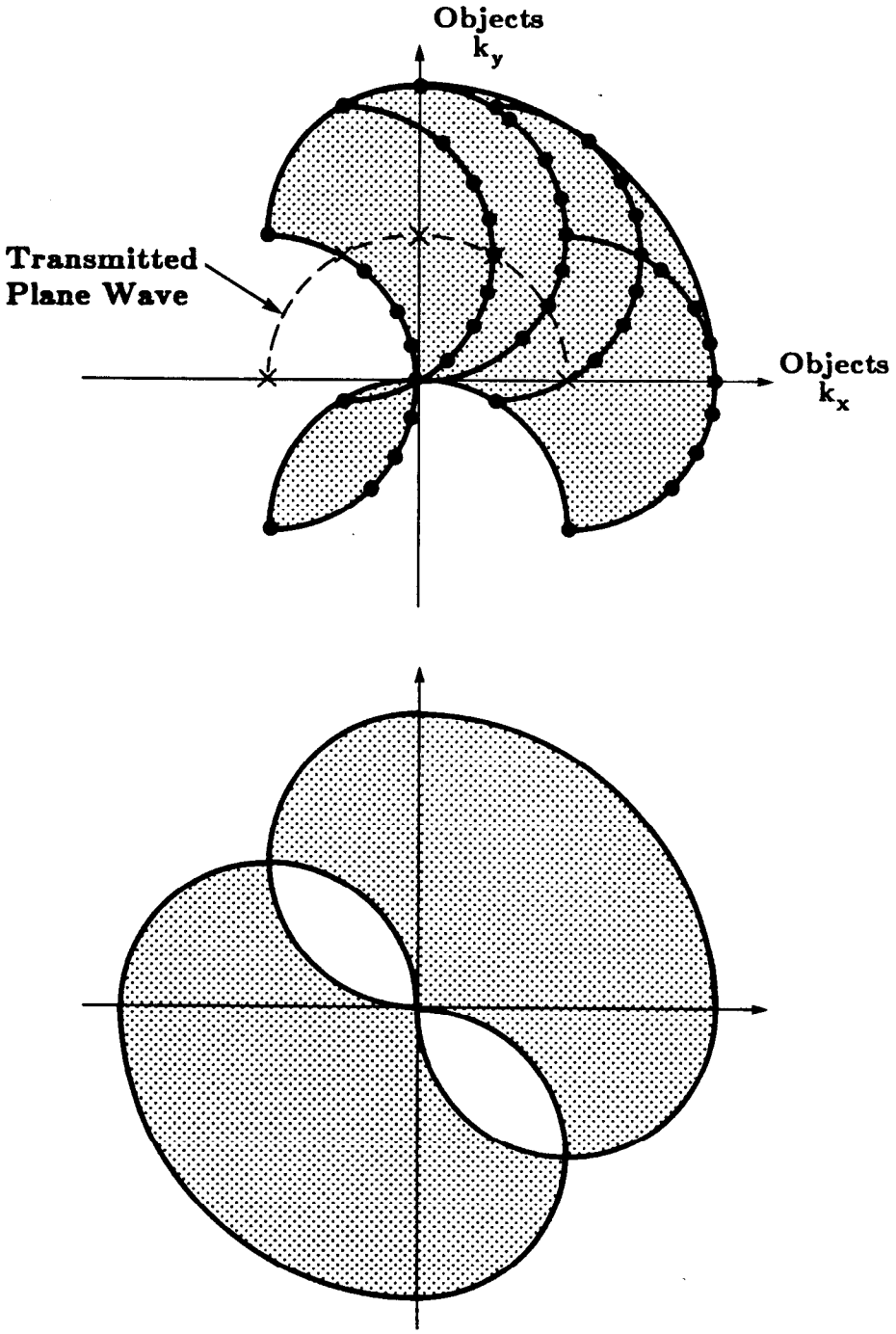


Figure 3.12 Estimate of the Fourier transform of an object are available in the shaded region for a VSP experiment (a). If, in addition, the object is real valued then the symmetry of the Fourier transform can be used to get the coverage shown in (b).

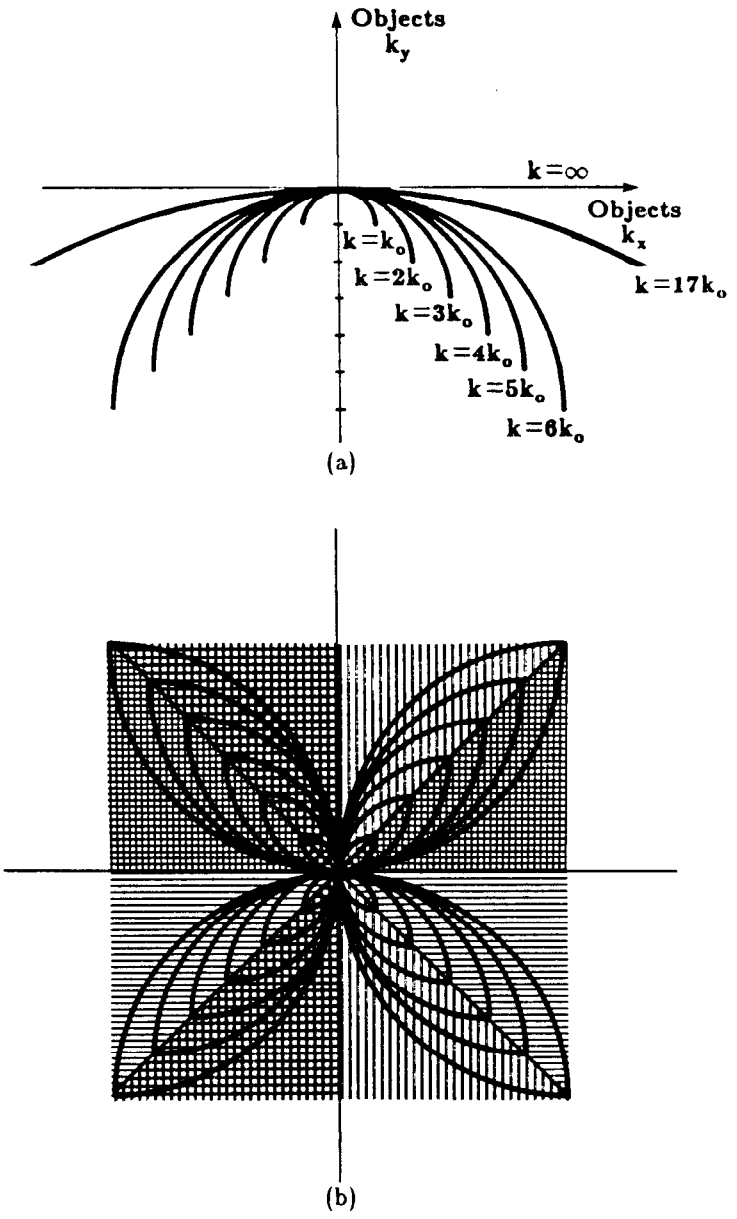


Figure 3.13 One view of a broadband diffraction tomography experiment will generate estimates of the object along the arcs in (a). With four views of the object complete coverage can be obtained as shown in (b).

## References


[Car70] William H. Carter, "Computational reconstruction of scattering objects from holograms," *Journal of the Optical Society of America,* Vol. 60, March 1970, pp. 306-314.

[Car74] W. H. Carter and P. C. Ho, "Reconstruction of inhomogeneous scattering objects from holograms," *Applied Optics,* Vol. 13, January 1974, pp. 162-172.

[Car76] P. L. Carson, T. V. Oughton, and W. R. Hendee, "Ultrasound transaxial tomography by reconstruction," in *Ultrasound in Medicine II,* D. N. White and R. W. Barnes, eds., Plenum Press, 1976, pp. 391-400.

[Dev82] A. J. Devaney, "A filtered backpropagation algorithm for diffraction tomography," *Ultrasonic Imaging,* Vol. 4, 1982, pp. 336-350.

[Dev84] A. J. Devaney, "Geophysical diffraction tomography," *IEEE Transaction Geological Science, Special Issue on Remote Sensing,* Vol. GE-22, January 1984, pp. 3-13.

[Goo68] J. W. Goodman, *Introduction to Fourier Optics,* McGraw Hill Book Company, San Francisco, 1968.

[Gre78] J. F. Greenleaf, S. K. Kenue, B. Rajagopalan, R. C. Bahn, and S. A. Johnson, "Breast imaging by ultrasonic computer-assisted tomography," in *Acoustical Imaging,* A. Metherell, ed., Plenum Press, 1978.

[Kak84] A. C. Kak, "Tomographic imaging with diffracting and non-diffracting sources," in *Array Processing Systems,* Simon Haykin, ed., Prentice Hall, 1984.

[Kav82] M. Kaveh, M. Soumekh, and R. K. Mueller, "Tomographic imaging via wave equation inversion," *ICASSP 82,* May 1982, pp. 1553-1556.

[Ken82] S. K. Kenue and J. F. Greenleaf, "Limited angle multifrequency diffraction tomography," *IEEE Transactions on Sonics and Ultrasonics,* Vol. SU-29, July 1982, pp. 213-217.

[LuZ84] Z. Q. Lu, M. Kaveh, and R. K. Mueller, "Diffraction tomography using beam waves: Z-average reconstruction," *Ultrasonic Imaging,* Vol. 6, January 1984, pp. 95-102.

[Mor53] Philip M. Morse and Herman Feshbach, *Methods of Theoretical Physics,* McGraw Hill Book Company, New York, 1953.

[Mue79] R. K. Mueller, M. Kaveh, and G. Wade, "Reconstructive tomography and applications to ultrasonics," *Proceedings of the IEEE,* Vol. 67, 1979, pp. 567-587.

[Nah82] D. Nahamoo and A. C. Kak, *Ultrasonic diffraction imaging,* TR-EE 82-20, School of Electrical Engineering, Purdue University, 1982.

[Nah84] D. Nahamoo, S. X. Pan, and A. C. Kak, "Synthetic aperture diffraction tomography and its interpolation-free computer implementation," *IEEE Transactions on Sonics and Ultrasonics,* Vol. SU-31, July 1984, pp. 218-229.

[Wol69] E. Wolf, "Three-dimensional structure determination of semi-transparent objects from holographic data," *Optics Communications,* Vol. 1, 1969, pp. 153-156.